Soft Matter

PAPER

View Article Online
View Journal | View Issue

Cite this: *Soft Matter*, 2017, 13, 4661

Orientation and crystallization of regioregular poly(3-dodecylthiophene) in alumina nanopores†

Hui Wu,*[ab] Yuji Higaki,[acd] Shiki Nojima[d] and Atsushi Takahara *[acd]

Received 30th April 2017,
Accepted 13th June 2017

DOI: 10.1039/c7sm00859g

rsc.li/soft-matter-journal

The orientation and crystallization of regioregular poly(3-dodecylthiophene) (P3DDT) in different diameter nanopores were investigated. P3DDT nanowires were prepared by a melt–wetting nonporous alumina template with P3DDT melts. The microstructure of the nanowires was analyzed by micro-Fourier transform infrared spectroscopy, grazing incidence wide angle X-ray diffraction, and differential scanning calorimetry. Although Form I modification prevails in all the nanowires, Form I crystals decrease and Form II crystals increase as the pore diameter decreases. The crystallites developed in the nanowires preferentially aligned with π–π stacking (*b*-axis) along the long axis of the wire and this orientation is marked as the wire diameter decreases. These results could provide guidance on designing polymeric nanomaterials for functional nanodevices in high performance organic photovoltaic cells, sensors, and electrodes.

Introduction

In recent years, π-conjugated polymers, especially poly(3-alkylthiophene)s (P3ATs), have received increasing attention in organic field effect transistors (OFETs) and organic solar cells (OSCs) due to their facile processability, high charge-carrier mobility and environmental stability.[1] P3ATs exhibit rich morphologies and properties depending on the side chain arrangement, *i.e.* regioregularity, and side chain length.[2–11] Because the physicochemical properties of materials strongly depend on their internal supramolecular organization, the morphology control, such as thermal[12] or solvent[13] treatment, has been introduced to modulate the ordering and phase separation of P3ATs to produce high performance devices.

One-dimensional (1-D) polymeric nanomaterials with a high aspect ratio have drawn significant attention because of the various attractive properties and their enormous potential applications.[14–43] Anodic aluminum oxide (AAO) is a metal oxide template consisting of well-ordered straight separated cylindrical nanopores. It offers an effective and convenient opportunity to prepare 1-D polymer nanomaterials with various diameters. The fabrication processes, such as annealing temperature and pore diameter, are commonly regulated to control the final 1-D nanostructures. With the aid of templates, ordered nanostructures with specific orientation were generated.[17–32]

The 1-D nanostructures can increase the surface area and ordering of P3ATs, and thus enhance the optoelectronic, electrochromic, and sensing properties. The well-aligned nanomaterial array produced by the AAO templates on a conducting substrate is an ideal structure for the active layer of high performance organic photovoltaic cells, sensors and electrochromic devices.[28–36] For instance, the poly(3-hexylthiophene) (P3HT) chains inside the nanorods oriented in the direction normal to the AAO pore wall and this crystalline orientation enhanced the nanorod electrical conductivity up to ten times of a continuous P3HT film.[28] The P3HT nanorod array provides a large interfacial area between the donor and the acceptor, shortens the transporting pathway of the charge carriers and hence enhances the photovoltaic device efficiency.[26,27]

Poly(3-dodecylthiophene) (P3DDT) is one of the promising P3ATs with good electrical properties, amazing polymorphs and complicated structural evolution. Although the nanoconfinement effect on the preferential orientation of the P3AT lamella crystals has been the subject of many studies,[28–32] the preferential orientation of P3DDT confined in nanopores has not been explored extensively. There is a stringent need to control the orientation and crystallization of conjugated polymers in 1-D nanostructures to fabricate high performance devices. In the present study, we prepared the P3DDT nanowires with different diameters by melt–wetting nanoporous AAO templates with polymer melts, and the orientation and crystalline structure of P3DDT nanowires are demonstrated by micro-Fourier transform

[a] *Institute for Materials Chemistry and Engineering, Kyushu University, Fukuoka 819-0395, Japan. E-mail: takahara@cstf.kyushu-u.ac.jp*
[b] *College of Material Engineering, Fujian Agriculture and Forestry University, Fuzhou 350002, China. E-mail: wuhuifafu@163.com*
[c] *International Institute for Carbon-Neutral Energy Research (WPI-I2CNER), Kyushu University, Fukuoka 819-0395, Japan*
[d] *Graduate School of Engineering, Kyushu University, Fukuoka 819-0395, Japan*

† Electronic supplementary information (ESI) available. See DOI: 10.1039/c7sm00859g

infrared spectroscopy (micro-FTIR) and grazing wide-angle incidence X-ray diffraction (GIWAXD).

Experimental

Sample preparation

Regioregular P3DDT with a molecular weight (M_n) of 41 600 and a polydispersity of 2.19 (determined by gel permeation chromatography using polystyrene standards) was purchased from Aldrich. The AAO templates with pore diameters of 300, 65, and 35 nm were prepared by a two-step electrochemical anodization process.[44] The SEM images of the AAO templates with pore diameters of 35, 65, and 300 nm are shown in Fig. 1.

P3DDT melts were infiltrated into the AAO template by placing a porous AAO template on top of a 150 μm thick P3DDT film under vacuum for 4 h at 468 K, which is well above the melting temperature of P3DDT at 425 K. The crystallization temperature of P3DDT measured by DSC is about 384 K and the crystallization rate of P3DDT is quite fast ($t_{1/2}$ = 2.2 min at 388 K);[45] the polymer/AAO assembly was crystallized at 388 K for 2 h to make the polymer crystal develop well in the nanopores, and was subsequently quenched in ice water quickly. Thin slices of the P3DDT film with protruding nanowires for SEM and micro-FTIR measurements were obtained by cutting the sample along the wire direction using a razor blade after removal of the AAO template using a phosphoric acid solution. To prepare the samples for XRD and DSC measurements, the bulk film under the AAO templates was removed using sharp blades. The residue on the template surface was further cleaned by wiping the template surface with cotton swabs wetted with $CHCl_3$ repeatedly until the cotton swabs turned colorless.

Characterization

The AAO templates and P3DDT nanowires were coated with a thin layer of osmium and examined by field emission scanning electron microscopy (Hitachi SU8000) with an accelerating voltage of 5 kV. Micro-Fourier transform infrared spectroscopy (micro-FTIR) measurements of the thin slices of the P3DDT nanowire/film were performed on a PerkinElmer FTIR spectrometer (Spectrum One) in connection with a microscope equipped with a MCT detector operating in the transmission mode. The IR beam was trimmed to 200 × 50 μm^2 by aperture. Polarized FTIR spectra were recorded using a wire-grid polarizer parallel or perpendicular to the long length of the P3DDT nanowire. 128 scans were integrated at a resolution of 2 cm^{-1} for each spectrum. The IR region at 870–790 cm^{-1} was analyzed using OPUS software, and the curve fittings were performed following the literature procedure.[4] The resultant band frequency and bandwidths were fixed parameters, while the intensity and band shape were variable parameters.

Grazing incidence X-ray diffraction (GIWAXD) measurements were carried out at the BL03XU beam line of SPring-8 (Japan Synchrotron Radiation Research Institute, Hyogo, Japan).[46,47] The incident X-ray wavelength, λ, was set to 0.100 nm. The X-ray incident angle (α_i) was 0.2°, which is above the critical angle (α_c) of P3DDT ($\alpha_{c,P3DDT}$ = 0.1°). The sample-to-detector distance was 450 mm calibrated with cerium oxide diffractions. Two-dimensional GIWAXD images were acquired using an imaging plate (IP) (Rigaku, Tokyo, Japan; R-AXIS IV++) with a resolution of 3000 × 3000 pixels (pixel size: 100 μm × 100 μm).

Thermal analysis of P3DDT within different nanopores was performed using a differential scanning calorimeter (Perkin-Elmer Inc., Waltham, MA; Diamond DSC) under a N_2 atmosphere. Four stacked P3DDT/AAO disks were sealed in aluminum pans. The scans were taken from 293 to 473 K with heating and cooling rates of 10 K min^{-1}.

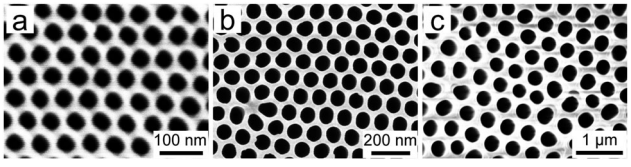

Fig. 1 SEM images of AAO templates with pore diameters of (a) 35 nm, (b) 65 nm, and (c) 300 nm.

Results and discussion

P3DDT nanowires were prepared by melt–wetting the porous AAO template with polymer melts. The thermal stability and mechanical rigidity of the alumina wall provide a strictly cylindrical constrained environment to fabricate 1-D polymer nanostructures. The polymers in the melt state are spontaneously wetted on the wall of the nanopores having a high surface energy. A capillary rise of P3DDT melts into the cylindrical nanopores leads to the formation of polymer nanowires.[18] Fig. 2A shows a SEM image of the parallel aligned P3DDT nanowire array after removal of the AAO template. The nanowires aligned normal to the bulk film surface.

Micro-FTIR[20,22] was applied to characterize the thin slices of the P3DDT nanowire/bulk film obtained by cutting the sample along the wire direction. The length of the nanowires is about 110 μm. The IR spectra were obtained by focusing the IR beam on the wire array and the bulk film with an aperture size of 200 × 50 μm^2.

The C_β–H (the hydrogen atom is attached to the thiophene ring) out-of-plane bending ($\delta(C_\beta–H)$) band at 870–790 cm^{-1} contains rich information about multiple microstructures of P3ATs.[4,9] It is known that the 819 cm^{-1} band is characteristic of the Form I crystalline phase; the component at 827 cm^{-1} is assigned to the Form II modification; 836 cm^{-1} is ascribed to the disordered phase where both the main chains and side chains are disordered; and 806 cm^{-1} is ascribed to an intermediate phase with twisted main chains and ordered side chains.[3] Fig. 2B shows the micro-FTIR spectra of P3DDT nanowires with diameters of 35, 65, 300 nm, and the bulk film in the region 870–790 cm^{-1}. To verify the components in the samples, the second derivative spectrum of the bulk film was obtained, as shown in Fig. S1 (ESI†). Four bands are identified at 819, 827, 836, and 806 cm^{-1}. The appearance of the 819 cm^{-1} band shows that the P3DDT bulk film contains Form I crystals.

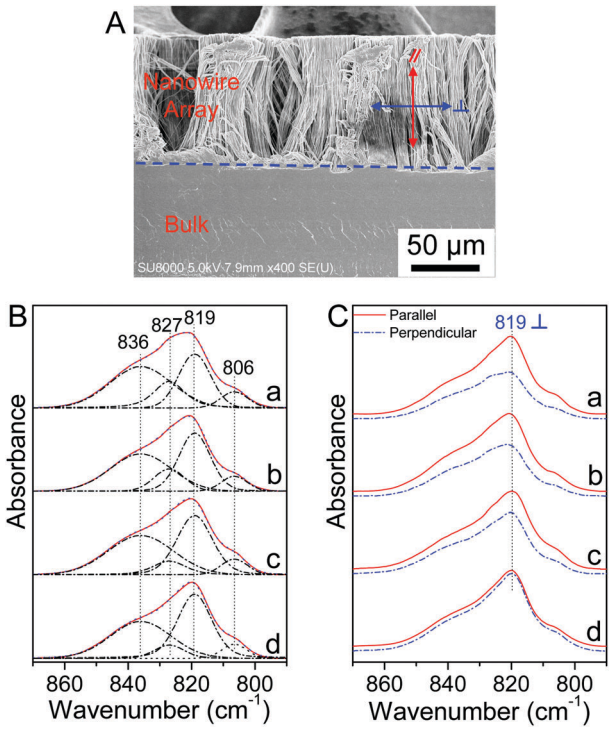

Fig. 2 (A) SEM image of a thin slice of the P3DDT nanowire/film. (B) Micro-FTIR spectra of the nanowire array with diameters of (a) 35 nm, (b) 65 nm, (c) 300 nm, and (d) bulk film. (C) Corresponding polarized micro-FTIR spectra: parallel polarization (—); perpendicular polarization (---) with respect to the wire length direction.

However, besides the 819 cm^{-1} band, a small 827 cm^{-1} band also can be distinguished in the second derivative spectrum. This indicates that the samples contain Form II crystals. Form I was found in most occasions, whereas Form II was discovered under more special preparation conditions, for example, by casting a P3DDT film from a xylene solution at room temperature and slow evaporation of the solvent.[2] Upon heating in most P3ATs, Form II transforms into Form I irreversibly at a temperature lower than its melting point.[2] Form I of P3DDT is the kinetically favored polymorph, while Form II is thermodynamically more stable at room temperature, but its formation is kinetically hindered.[5] In our samples, even for the bulk film crystallized from melt, small amounts of Form II modification exist.

The relative amount of crystalline fractions for a semicrystalline polymer can be simply described by the crystallinity index,[48] which can be expressed as

$$C_{819} = \frac{A_{819}}{A_{819} + A_{827} + A_{836} + A_{806}} \times 100\%$$

$$C_{827} = \frac{A_{827}}{A_{819} + A_{827} + A_{836} + A_{806}} \times 100\%$$

$$C_{806} = \frac{A_{806}}{A_{819} + A_{827} + A_{836} + A_{806}} \times 100\%$$

where C_{819}, C_{827}, and C_{806} represent the crystallinity index of Form I crystals, Form II crystals, and the intermediate phase, A_{819}, A_{827}, A_{836}, and A_{806} are the respective band areas for the bands at 819, 827, 836, and 806 cm^{-1}, respectively. Curve fitting was used to decompose the overlapped bands.

Table 1 Crystallinity index of Form I, Form II, and the intermediate phase indexed as C_{819}, C_{827} and C_{806}

	C_{819}	C_{827}	C_{806}
35 nm	31 ± 3	17 ± 3	7 ± 0.8
65 nm	36 ± 3	14 ± 2	7 ± 0.3
300 nm	41 ± 2	10 ± 1	8 ± 0.8
Bulk	45 ± 1	9 ± 1	7 ± 0.4

As shown in Table 1 for the three respective samples, the average C_{819} is much higher than C_{827}, indicating that Form I dominates the crystals in all the samples. No appreciable change in the intermediate phase is detectable as the wire diameter varies. Form I crystals decrease and Form II crystals increase as the wire diameter decreases.

Form II is a structure with side chain interdigitation, while Form I is a non-interdigitated structure.[2] The major difference between Form I and Form II is characterized by different layer spacings with the number of carbon atoms in the side chains.[6] The layer period (*a*-axis direction) of Form I (2.58 nm)[7] is larger than that of Form II (1.98 nm).[2] Due to the stronger confinement, Form II crystals with shorter layer period are more favorable in the smaller nanowires than those in the larger ones. Since Form II is more likely found in P3ATs with longer alkyl side chains,[8] it is predicable that P3ATs bearing longer alkyl side chains contain more Form II crystals in nanoconfinement.

To assess the chain orientation of the crystalline domains in nanowires, polarized FTIR spectroscopy was then applied. The growth direction of nanowires was defined as the reference direction, and polarized FTIR spectra were recorded using a wire-grid polarizer parallel or perpendicular to the wire direction (Fig. 2A). Fig. 2C shows the polarized micro-FTIR spectra. The transition moment of the $\delta(C_\beta\text{–H})$ mode for the band at 819 cm^{-1} is approximately normal to the thiophene ring planes.[9,49] Hence, the 819 cm^{-1} band can be used to probe the orientation direction of thiophene ring planes (π–π stacking direction) in the nanopores. The solid lines are the spectra in the parallel polarization, whereas the dashed lines represent the perpendicular spectra. For the nanowires, the intensity of the 819 cm^{-1} band in the parallel spectrum is stronger than that in the perpendicular one. This indicates that the thiophene ring planes in the nanowires are preferentially aligned perpendicular to the wire growth direction and the π–π stacking direction (*b*-axis) of the crystallites is aligned parallel to the wire direction. The conjugated backbone adopts a face-on orientation along the wire direction.

The dichroic ratio of the 819 cm^{-1} band was calculated as $R = A_{\parallel}/A_{\perp}$, where $A_{\parallel}$ and $A_{\perp}$ are the curve-fitting absorbance (peak area) for electric vector parallel and perpendicular to the wire direction, respectively. The dichroic ratio of the 819 cm^{-1} band in the nanowires with diameters of 35 nm, 65 nm, and 300 nm, and the bulk film is 1.85 ± 0.09, 1.66 ± 0.01, 1.45 ± 0.02, and 0.98 ± 0.03, respectively. This result shows that the π–π stacking along the wire direction increases as the wire diameter decreases.

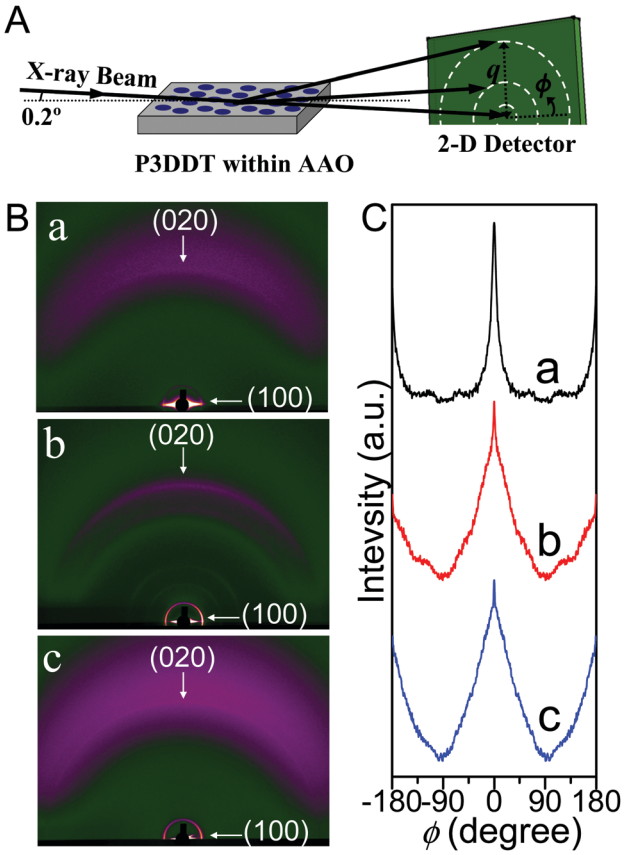

Fig. 3 (A) Schematic illustration of the GIWAXD geometry employed for investigating the P3DDT within the nanopores. (B) 2-D GIWAXD patterns and (C) azimuthal intensity distribution of the (100) reflection in nanowire arrays of (a) 35 nm, (b) 65 nm, and (c) 300 nm.

GIWAXD measurements (Fig. 3A) were used to determine the ordering of the crystals in the nanostructures. Fig. 3B shows the two-dimensional (2-D) GIWAXD patterns of nanowire arrays within nanopores of 35 nm, 65 nm, and 300 nm. The AAO templates have amorphous structure. Referring to the orthogonal unit cell (a = 2.583 nm, b = 0.775 nm and c = 0.777 nm) of Form I crystals of P3DDT,[7] the reflections located at the scattering vector (q) values of 2.3 and 16.4 nm^{-1} are indexed as (100) and (020), respectively. Also, the second order (200) and the third order (300) planes are visible in the 1-D XRD profiles extracted from the azimuthal integration of the 2-D diffraction patterns, as shown in Fig. S2 (ESI†). The (100) reflection is associated with the side-by-side arrangement of the main chains and the (020) reflection arises from the π–π stacking of conjugated aromatic rings. The strongest intensity of the (100) reflection is located on the equator and that of the (020) reflection is on the meridian, indicating that the a-axis of the crystals is highly aligned perpendicular to the long axis of the wire and the b-axis is parallel to the wire. The face-on crystal structure along the wire direction is prevalent in all the nanowires.

To evaluate the crystal orientation, the full width at half-maximum (FWHM) of the (100) reflection with distinguishable intensity in nanowires was analyzed. Fig. 3C shows the integrated intensities of (100) diffraction against azimuthal angle ϕ ($\phi = 0^\circ$ corresponds to the equator) in the range of −180 to 180° exhibited according to the symmetry of profiles. The FWHM values of 35 nm, 65 nm, and 300 nm nanowires are 12.6, 45.2, and 59.7, respectively. The FWHM value increases as the wire diameter increases, implying that the alignment of P3DDT crystals in smaller nanowires is considerably improved than that in the larger ones due to the stronger confinement. This confirms that the smaller pore has a profound confinement effect on the crystallite orientation, which is in accordance with the IR results.

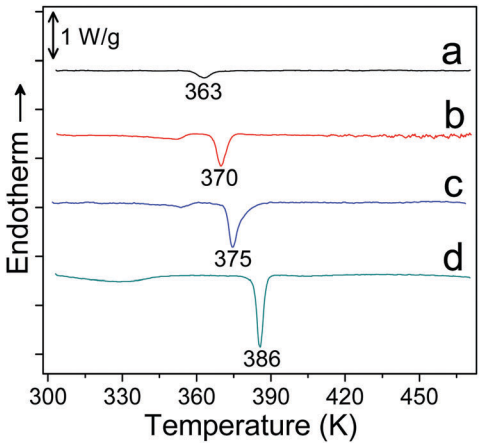

Fig. 4 DSC scans of P3DDT nanostructures crystallized at a cooling rate of 10 K min^{-1} within templates of (a) 35 nm, (b) 65 nm, (c) 300 nm, and (d) bulk film.

To analyze the nucleation behavior of the aligned P3DDT nanostructures inside porous alumina, DSC scans of P3DDT nanostructures were performed. Fig. 4 shows DSC scans on cooling. Bulk P3DDT shows a strong exothermic crystallization peak at 386 K. The traces of P3DDT in self-ordered AAO are distinctly different. In AAO with pore diameters of 300, 65, and 35 nm the exothermic peak is shifted to 375, 370, and 363 K, respectively. The crystallization temperature in smaller nanopores is significantly lower than that in the larger ones and it needs much larger supercooling for crystallization. This indicates that the nucleation is suppressed as the wire diameter decreases, which is in agreement with the reported results.[17,50]

It is well known that the alumina surface improves the ordering of P3HT nanostructures.[28–30] The P3HT chains inside the nanorods align in the direction normal to the AAO pore wall, and the π–π stacking of P3HT lamellae is parallel to the rod[28] or tube[30] axis. To minimize the contact of the hydrophobic dodecyl side chains to the hydrophilic alumina, the P3DDT chains in contact with the alumina surface would align normal to the AAO pore wall. This will facilitate the arrangement of P3DDT chains orientated with the face-on conformation along the wire axis.

If the nanostructures were connected with a bulk reservoir, bulk crystallization dominates the crystallization of nanowires.[17,22] Because the crystallization temperature of nanostructures is lower than that of the bulk film, the crystals formed in the bulk act as nuclei to initiate the crystallization of P3DDT nanowires.[17,22]

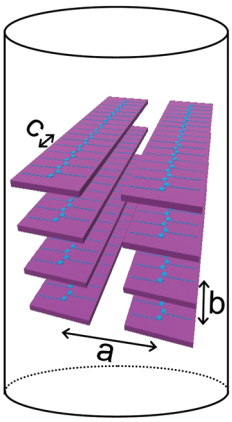

Fig. 5 Schematic illustration of the P3DDT lamellae developed in AAO nanopores with π–π stacking along the wire direction.

The well-aligned crystallites grow in the nanowires, while other growth directions are constrained due to cylindrical confinement of the pore walls. The fast growth direction of P3DDT crystals is the π–π stacking direction (*b* axis).[6,8] A kinetic selection of crystallite growth compatible with the nanopores is favored, leading to π–π stacking in the nanowires having the face-on conformation along the wire axis. Due to the stronger confinement of smaller nanopores, the strict crystal growth in the smaller wires enhanced the crystal orientation. The schematic of P3DDT crystals developed in the nanopores is shown in Fig. 5.

Conclusions

This study examined the nanoconfinement effect on the microstructure of 1-D P3DDT nanowires by micro-FTIR, GIWAXD and DSC. The Form I crystals dominate the nanowires. As the nanowire diameter decreases, the Form I crystals decrease and Form II crystals increase. Due to the constrained crystallite growth in the nanopores, P3DDT lamellae developed in the nanopores take the orientation with π–π stacking along the wire direction, and this orientation increases as the pore diameter decreases. This result holds promise for the application of nanomaterials for highly efficient organic solar cells, sensors, and electrochromic devices.

Acknowledgements

This work was supported by the Photon and Quantum Basic Research Coordinated Development Program from the Ministry of Education, Culture, Sports, Science and Technology, Japan. This work was performed under the Cooperative Research Program of ''Network Joint Research Center for Materials and Devices''. The GIWAXD measurements were performed at BL03XU in SPring-8 with the approval of Japan Synchrotron Radiation institute (JASRI, proposal number: 2016A7211). We thank Dr Taizo Kabe for his assistance in the experiments on BL03XU. Dr Yasushi Okamoto and Mr Takashi Aoki (DENSO CORP) are also gratefully acknowledged for kindly providing the opportunity to conduct the GIWAXD measurements on the BL03XU. H. Wu thanks the Award Program for Minjiang Scholar Professorship, the Scientific Research Foundation for the Returned Overseas Chinese Scholars, State Education Ministry, and Training Fund for Outstanding Young Scholars of Fujian Agriculture and Forestry University (xjq201421) for support.

References

1 H. Sirringhaus, P. J. Brown, R. H. Friend, M. M. Nielsen, K. Bechgaard, B. M. W. Langeveld-Voss, A. J. H. Spiering, R. A. J. Janssen, E. W. Meijer, P. Herwig and D. M. de Leeuw, *Nature*, 1999, **401**, 685.
2 T. J. Prosa, M. J. Winokur and R. D. McCullough, *Macromolecules*, 1996, **29**, 3654.
3 Y. Guo, Y. Jin and Z. Su, *Soft Matter*, 2012, **8**, 2907.
4 K. Yazawa, Y. Inoue, T. Yamamoto and N. Asakawa, *J. Phys. Chem. B*, 2008, **112**, 11580.
5 Y. Guo, L. Wang, Y. Y. Han, Y. H. Geng and Z. H. Su, *Polym. Chem.*, 2014, **5**, 1938.
6 M. Brinkmann, *J. Polym. Sci., Part B: Polym. Phys.*, 2011, **49**, 1218.
7 K. Tashiro, K. Ono, Y. Minagawa, M. Kobayashi, T. Kawai and K. Yoshino, *J. Polym. Sci., Part B: Polym. Phys.*, 1991, **29**, 1223.
8 S. V. Meille, V. Romita, T. Caronna, A. J. Lovinger, M. Catellani and L. Belobrzeckaja, *Macromolecules*, 1997, **30**, 7898.
9 K. Yazawa, Y. Inoue, T. Yamamoto and N. Asakawa, *Phys. Rev. B: Condens. Matter Mater. Phys.*, 2006, **74**, 094204.
10 Y. Guo, Y. Jin and Z. Su, *Polym. Chem.*, 2012, **3**, 861.
11 V. Causin, C. Marega, A. Marigo, L. Valentini and J. M. Kenny, *Macromolecules*, 2005, **38**, 409.
12 L. H. Nguyen, H. Hoppe, T. Erb, S. Gunes, G. Gobsch and N. S. Sariciftci, *Adv. Funct. Mater.*, 2007, **17**, 1071.
13 G. H. Lu, L. G. Li and X. N. Yang, *Adv. Mater.*, 2007, **19**, 3594.
14 C. R. Martin, *Acc. Chem. Res.*, 1995, **28**, 61.
15 M. Steinhart, *Adv. Polym. Sci.*, 2008, **220**, 123.
16 H. Wu, J. Yang, S. Cao, L. Huang and L. Chen, *Macromol. Chem. Phys.*, 2014, **215**, 584.
17 M. Steinhart, P. Göring, H. Dernaika, M. Prabhukaran, U. Gösele, E. Hempel and T. Thurn-Albrecht, *Phys. Rev. Lett.*, 2006, **97**, 027801.
18 H. Wu, W. Wang, H. Yang and Z. Su, *Macromolecules*, 2007, **40**, 4244.
19 M. C. Garcia-Gutierrez, A. Linares, J. J. Hernandez, D. R. Rueda, T. A. Ezquerra, P. Poza and R. J. Davies, *Nano Lett.*, 2010, **10**, 1472.
20 H. Wu, Z. Su and A. Takahara, *Soft Matter*, 2011, **7**, 1868.
21 J. L. Lutkenhaus, K. McEnnis, A. Serghei and T. P. Russell, *Macromolecules*, 2010, **43**, 3844.
22 H. Wu, Z. Su and A. Takahara, *Soft Matter*, 2012, **8**, 3180.
23 Y. Guan, G. Liu, G. Ding, T. Yang, A. J. Mueller and D. Wang, *Macromolecules*, 2015, **48**, 2526.
24 H. Wu, Y. Cao, R. Ishige, Y. Higaki, T. Hoshino, N. Ohta and A. Takahara, *ACS Macro Lett.*, 2013, **2**, 414.

25 W. H. Liew, M. S. Mirshekarloo, S. T. Chen, K. Yao and F. E. H. Tay, *Sci. Rep.*, 2015, **5**, 9790.
26 X. L. Sun, Q. Q. Fang, H. H. Li, Z. J. Ren and S. K. Yang, *Langmuir*, 2016, **32**, 3269.
27 C.-L. Liu and H.-L. Chen, *Macromolecules*, 2017, **50**, 631.
28 J. S. Kim, Y. Park, D. Y. Lee, J. H. Lee, J. H. Park, J. K. Kim and K. Cho, *Adv. Funct. Mater.*, 2010, **20**, 540.
29 D. Chen, W. Zhao and T. P. Russell, *ACS Nano*, 2012, **6**, 1479.
30 J. Byun, Y. Kim, G. Jeon and J. K. Kim, *Macromolecules*, 2011, **44**, 8558.
31 J. Martin, M. Campoy-Quiles, A. Nogales, M. Garriga, M. I. Alonso, A. R. Goni and M. Martin-Gonzalez, *Soft Matter*, 2014, **10**, 3335.
32 A. Santos, P. Formentín, J. Pallarés, J. Ferré-Borrull and L. F. Marsal, *Sol. Energy Mater. Sol. Cells*, 2010, **94**, 1247.
33 Y. Yang, K. Mielczarek, A. Zakhidov and W. Hu, *ACS Appl. Mater. Interfaces*, 2016, **8**, 7300.
34 K. M. Coakley, B. S. Srinivasan, J. M. Ziebarth, C. Goh, Y. X. Liu and M. D. McGehee, *Adv. Funct. Mater.*, 2005, **15**, 1927.
35 T. Kim, H. Yoon, H. J. Song, N. Haberkorn, Y. Cho, S. H. Sung, C. H. Lee, K. Char and P. Theato, *Macromol. Rapid Commun.*, 2012, **33**, 2035.
36 C. W. Chu, K. S. Jeng, M. H. Chi, C. C. Tsai, M. H. Cheng and J. T. Chen, *Macromol. Chem. Phys.*, 2016, **217**, 2074.
37 K. Shin, H. Q. Xiang, S. I. Moon, T. Kim, T. J. McCarthy and T. P. Russell, *Science*, 2004, **306**, 76.
38 P. Huang, Y. Guo, R. P. Quirk, J. J. Ruan, B. Lotz, E. L. Thomas, B. S. Hsiao, C. A. Avila-Orta, I. Sics and S. Z. D. Cheng, *Polymer*, 2006, **47**, 5457.
39 S. Nakagawa, H. Marubayashi and S. Nojima, *Eur. Polym. J.*, 2015, **70**, 262.
40 X. Dai, J. Niu, Z. Ren, X. Sun and S. Yan, *J. Phys. Chem. B*, 2016, **120**, 843.
41 M. H. Cheng, H. W. Ko, P. Y. Chung, C. W. Chang and J. T. Chen, *Soft Matter*, 2016, **12**, 8087.
42 J. Xue, Y. Xu and Z. Jin, *Langmuir*, 2016, **32**, 2259.
43 B. Sanz, C. von Bilderling, J. S. Tuninetti, L. Pietrasanta, C. Mijangos, G. S. Longo, O. Azzaroni and J. M. Giussi, *Soft Matter*, 2017, **13**, 2453.
44 H. Masuda and K. Fukuda, *Science*, 1995, **268**, 1466.
45 S. L. Liu and T. S. Chung, *Polymer*, 2000, **41**, 2781.
46 H. Masunaga, H. Ogawa, T. Takano, S. Sasaki, S. Goto, T. Tanaka, T. Seike, S. Takahashi, K. Takeshita, N. Nariyama, H. Ohashi, T. Ohata, Y. Furukawa, T. Matsushita, Y. Ishizawa, N. Yagi, M. Takata, H. Kitamura, K. Sakurai, K. Tashiro, A. Takahara, Y. Amamiya, K. Horie, M. Takenaka, T. Kanaya, H. Jinnai, H. Okuda, I. Akiba, I. Takahashi, K. Yamamoto, M. Hikosaka, S. Sakurai, Y. Shinohara, A. Okada and Y. Sugihara, *Polym. J.*, 2011, **43**, 471.
47 H. Ogawa, H. Masunaga, S. Sasaki, S. Goto, T. Tanaka, T. Seike, S. Takahashi, K. Takeshita, N. Nariyama, H. Ohashi, T. Ohata, Y. Furukawa, T. Matsushita, Y. Ishizawa, N. Yagi, M. Takata, H. Kitamura, A. Takahara, K. Sakurai, K. Tashiro, T. Kanaya, Y. Amemiya, K. Horie, M. Takenaka, H. Jinnai, H. Okuda, I. Akiba, I. Takahashi, K. Yamamoto, M. Hikosaka, S. Sakurai, Y. Shinohara, Y. Sugihara and A. Okada, *Polym. J.*, 2013, **45**, 109.
48 S. Krimm and A. V. Tobolsky, *J. Polym. Sci.*, 1951, **7**, 57.
49 T. Mizokuro, Y. Okamoto, C. Heck, H. Aota and N. Tanigaki, *J. Appl. Polym. Sci.*, 2014, **131**, 40136.
50 H. Duran, M. Steinhart, H. J. Butt and G. Floudas, *Nano Lett.*, 2011, **11**, 1671.

